Comparison of dynamic light scattering measurements and mode-coupling theory for the tagged particle dynamics of a hard-sphere suspension

W. van Megen
Department of Applied Physics, Royal Melbourne Institute of Technology, Melbourne, Victoria 3000, Australia
(Received 29 May 2007; published 5 December 2007)

The mean-squared displacement, velocity autocorrelation function, and the non-Gaussian parameter, obtained by dynamic light scattering on suspensions of particles with hard-sphere interactions, are compared with the results of the idealized version of mode-coupling theory. Both leading order asymptotic and full numerical solutions of the mode-coupling equations are considered. Experiment and the full numerical results of the theory expose similar qualitative changes at the volume fraction of the first order freezing transition. In particular, the emergence of negative algebraic decays in the velocity autocorrelation function of the undercooled suspension suggest the emergence of clusters in which particles are trapped. Consistency of experiment, computer simulation, and theory in this regard suggests that, at particular strengths of the delayed, nonlinear feedback, contained in mode coupling theory, the latter predicts not only structural arrest which, as already established, is symptomatic of a glass transition, but also a more subtle change in dynamics that signals the onset of the first order transition.

DOI: 10.1103/PhysRevE.76.061401 PACS number(s): 82.70.Dd, 64.70.Pf, 61.20.Ne

I. INTRODUCTION

Considerable experimental and theoretical effort has been, and continues to be, directed towards an explanation for the dramatic increase in the structural relaxation time and resistance to flow of a liquid when undercooled. Many liquids, when cooled very quickly below a certain temperature, attain an apparent viscosity so large that they behave like brittle solids. In these amorphous solids, or glasses, the structural rearrangements, that with slower cooling might have effected a first order transition into a crystalline solid, are effectively frustrated.

Interest in this aspect of condensed matter has intensified since it was discovered, about two decades ago [1], that mode-coupling theory (MCT) applied to very dense fluids yields a dynamical singularity that has been identified with the glass transition (GT). A comprehensive review of the theory [2] opens as follows: "The mode-coupling theory for the density-fluctuation dynamics was developed originally in order to deal with the cage effect." The microscopic picture, first introduced by Frenkel [3], proffered by this is that atoms of a liquid move spontaneously from one neighbor cage to another. The entrapment time lengthens on increasing the liquid's density, or decreasing its temperature, to the point of solidification where atoms become permanently trapped in their respective neighbor cages. So the entrapment time can be considered as a crossover from local solidity to fluidity in which sense the cage picture, as its proponent suggests, offers a microscopic description of Maxwell's model of viscoelasticity [4]. Obviously, this model does not distinguish between crystallinity and amorphousness. MCT [1,2] goes beyond the ideas of Maxwell and Frenkel in that the delayed nonlinear coupling between density fluctuations, included in the theory, attempts to describe the cooperation, or backflow, required for an atom to leave its neighbor cage. The resulting theory describes the observed decay of the correlation of density fluctuations with quantitative accuracy [2], at least for those cases where the interactions between the fluid's particles are simple and static structure factors, the only input to the theory, are available. Moreover, since the structure factors that serve as initial conditions to the mode-coupling equations correspond to those of the fluid phase, the arrest of density fluctuations predicted by the theory necessarily signals solidification into an amorphous solid. Accordingly, the anomalously slow relaxation phenomena that emerge on cooling or densification of the fluid have been attributed solely to the glass transition rather the first order freezing transition.

A colloidal suspension of particles with hard-sphere-like interactions is one system for which MCT has turned out to be particularly successful [2]. This system has a freezing-melting transition that can be mapped onto that known for the hard sphere system, and a glass transition [5,6]. A small spread in particle radii delays nucleation [7] of the crystalline phase sufficiently to allow the dynamics and structure of the metastable, or undercooled, suspension to be measured without actually losing sight of the equilibrium phase boundary. Both the coherent and self-intermediate scattering functions, respectively, expressing the time correlation function of particle number density fluctuations and the moment generating function of the particle displacements, have been measured on this system by dynamic light scattering (DLS) and analyzed by MCT [8–10]. To place the theory's success in its description of these observations in perspective, it must be mentioned that, since to date they have generally been based on the asymptotic solutions to the idealized MCT equation, comparisons with experiment have been restricted to volume fractions in the vicinity of the observed GT.

More recent DLS experiments [11,12] and molecular dynamics (MD) computer simulations [13], respectively on colloidal and ballistic hard spheres, have exposed qualitative differences in some dynamical properties between the thermodynamically stable ($\varphi < \varphi_f$) and metastable ($\varphi_f < \varphi < \varphi_g$) systems of hard spheres. (Here the volume fractions $\varphi_f = 0.493$ and $\varphi_g \approx 0.57$ are, respectively, the freezing and glass transition volume fractions found for this system.) Negative

power-law decays of the velocity autocorrelation function are one distinguishing feature of the metastable fluid [12,13]. Such decays are redolent of the classical Lorentz gas [14] and suggest that some of the particles are trapped and, therefore, unable to dissipate completely the fluctuating thermal forces. In the linear hydrodynamic regime thermal fluctuations dissipate by propagating longitudinal and diffusing transverse momentum currents—respectively sound and viscous flow. It is, therefore, of some significance that MD simulations [13] find that the amplitude of the classical (positive) $\tau^{-3/2}$ hydrodynamic "tail" of the velocity autocorrelation function (VAF) [15–17]—the manifestation of diffusing transverse modes—goes to zero as the fluid's volume fraction approaches φ_f from below. The idealized version of MCT [2] considers thermal forces as white noise, i.e., shear modes are neglected and longitudinal modes are presumed to propagate instantaneously. The consistency between this version of the theory and experiments, mentioned above, suggest that this commonly applied decoupling of the particles' momenta and positions [18] is not without merit, at least for a suspension of hard spheres.

The comparison between the results of DLS experiments and MCT, in this paper, goes beyond the studies mentioned above in several respects; first, in addition to the mean-squared displacement, the velocity autocorrelation function and the non-Gaussian parameter are considered; second, the range of volume fractions studied extends down to very low values; and third, both full numerical solutions and the asymptotic solutions to the MCT [19,20] equations are used in the comparison. While MCT supposedly contains no *prima facie* information about the first order transition, the primary purpose here is, nonetheless, to see whether either solution exposes qualitative changes around this transition in any way similar to those found in experiment and computer simulation.

II. METHODS

A. Experiment

DLS measurements [11,21] were performed on a mixture of polymer and silica spheres, having the same average radius and coated with the same thin steric barrier. The refractive index of the suspending liquid was adjusted so that scattering from the structure and particle number density fluctuations was suppressed. Once this is achieved the fluctuations of the light scattered by the suspension are due entirely to the displacements of single (tagged) particles. The normalized autocorrelation function of the scattered light is then the self-intermediate scattering function (ISF),

$$F_s(q,\tau) = \langle \exp[i\mathbf{q}\cdot\Delta\mathbf{r}(\tau)]\rangle. \tag{1}$$

Here $\mathbf{q}$ is the wave vector and $\Delta\mathbf{r}(\tau)$ is the particle displacement in time τ. Further experimental details are documented in Refs. [11,21]. In the ensemble average, denoted by the angular brackets, the right-hand side of Eq. (1) can be expanded in terms of the even cumulants of the particle displacement distribution, as follows [22]:

$$\ln F_s(q,\tau) = -\frac{q^2}{6}\langle\Delta r^2(\tau)\rangle - \frac{1}{2}\left(\frac{q^2}{6}\right)^2\left[\frac{3}{5}\langle\Delta r^4(\tau)\rangle - \langle\Delta r^2(\tau)\rangle^2\right] + \cdots, \tag{2}$$

where the first (nonzero) cumulant, $\langle\Delta r^2(\tau)\rangle$, is the particle mean-squared displacement (MSD). The short and long time self-diffusion coefficients are defined by [18]

$$D_s = \lim_{\tau\to 0}\frac{\langle\Delta r^2(\tau)\rangle}{6\tau}, \quad D_l = \lim_{\tau\to\infty}\frac{\langle\Delta r^2(\tau)\rangle}{6\tau}, \tag{3}$$

where "0" and "∞" refer to the lower and upper limits of the experimental time window.

The rotationally invariant or Gaussian component of the tagged particle number density fluctuations, obtained in the limit $q\to 0$, is

$$F_s(q\to 0,\tau) = F_s^{(G)}(q,\tau) = \exp[-q^2\langle\Delta r^2(\tau)\rangle/6]. \tag{4}$$

The second cumulant, or non-Gaussian parameter,

$$\alpha(\tau) = \frac{3}{5}\langle\Delta r^4(\tau)\rangle - \langle\Delta r^2(\tau)\rangle^2, \tag{5}$$

expresses the first deviation from rotational invariance. This expression differs from that, $\alpha_2(\tau)=\alpha(\tau)/\langle\Delta r^2(\tau)\rangle^2$, usually employed to describe the leading order non-Gaussian effects [16,17]. The reason for the present choice is that division by $\langle\Delta r^2(\tau)\rangle^2$ compounds experimental noise and may obscure subtleties in the behavior for large delay times.

The point, (R_m^2,τ_m), where the deviation from Markovian particle displacements is greatest is that where the logarithmic slope of the MSD has its minimum value;

$$\nu = \min[d\log\langle\Delta r^2(\tau)\rangle/d\log\tau]. \tag{6}$$

As in previous work [11,12], ν will be referred to as the "stretching index."

The velocity autocorrelation function (VAF) [16],

$$Z(\tau) = \langle v(0)v(\tau)\rangle = -\lim_{q\to 0}\frac{1}{q^2}\frac{d^2}{d\tau^2}F_s(q,\tau) = \frac{d^2}{d\tau^2}\langle\Delta r^2(\tau)\rangle \tag{7}$$

is another quantity considered in detail.

After mapping the equilibrium phase behavior onto that known for the hard-sphere system [23], the suspension's freezing, melting and glass transition volume fractions are $\varphi_f=0.493$, $\varphi_m\approx 0.545$, and $\varphi_g\approx 0.565$, respectively [5,24]. Experimental data analyzed in terms of MCT below comprises the thermodynamically stable ($\varphi<\varphi_f$) and metastable ($\varphi_f<\varphi<\varphi_g$) suspensions. As discussed elsewhere [11], differential settling of the two types of particle over very long periods prevents acquisition of unambiguous data for $\varphi>\varphi_g$.

B. Mode coupling theory analysis

The starting point of the theory for a system with diffusive dynamics, characterized by the diffusion coefficient D_o, is the following formally exact expression for the self-ISF [19,20]:

$$\dot{F}_s(q,\tau) + D_o q^2 F_s(q,\tau) + D_o q^2 \int_0^\tau m_s(q,\tau-\tau')\dot{F}_s(q,\tau')d\tau' = 0. \tag{8}$$

The memory function used for studies of the GT is a quadratic functional of the coherent and self-ISFs, $m_s(q,\tau) = \mathcal{F}(F(q,\tau),F_s(q,\tau))$, which is completely specified by the static structure factor. These equations possess a dynamical singularity which, for the hard-sphere system, occurs at the volume fraction $\phi_c = 0.516$. At this point the solutions to Eq. (8) separate into those that decay to zero and those that do not; i.e., for $\phi < \phi_c$, $F_s(q,\tau\to\infty)=0$, while for $\phi > \phi_c$, $F_s(q,\tau\to\infty)0$. The volume fraction ϕ_c is defined in the theory as an ergodic to nonergodic transition and identified with the experimental GT.

For $\phi < \phi_c$ the leading order asymptotic solution to Eq. (8) separates the decay of $F_s(q,\tau)$ into the β and α processes. The crossover from the faster β process to the slower α process occurs at delay time τ_β and the amplitude, the Lamb-Mössbauer factor, $f(q)=F_s(q,\tau_\beta)$, is independent of φ. The α-process is characterized by a second scaling time, τ_α. These times scale with the separation parameter, $\varepsilon = 1 - \varphi/\varphi_c$, as follows:

$$\tau_\beta \sim \varepsilon^{-\delta},$$

$$\tau_\alpha \sim \varepsilon^{-\gamma}, \tag{9}$$

For the hard sphere system $\delta = 1.66$ and $\gamma = 2.58$. The particular values for these exponents and ϕ_c are obtained from the theory when the Percus-Yevick approximation is used for the structure factor. They show some variation with the particular form used for the structure factor [20].

The bulk of the analysis below employs full numerical solutions to the MCT equations [19,20,25]. To absorb the difference between the critical volume fraction, φ_c (=0.516), and the observed GT volume fraction, φ_g (≈0.565), as well as any experimental error in φ, fitting of the MCT result for a given dynamical property to the corresponding experimental result has previously [8,10] been done by treating the separation, ε, from the critical volume fraction as a free parameter. A second free parameter sets the microscopic time scale.

A slightly different approach is used here; the MCT volume fractions are scaled to the experimental ones by matching of the stretching indices of their respective MSDs. The microscopic time scale is set by the experimental value of the short-time self-diffusion coefficient, D_s. In the ensuing discussion the two classes of solutions to the MCT equations will simply be referred to as the numerical MCT and asymptotic MCT.

III. RESULTS AND DISCUSSION

A. Mean-squared displacements

In Fig. 1 stretching indices, ν, derived from the experimental data and numerical MCT, are set out against the respective experimental and MCT volume fractions. Note that

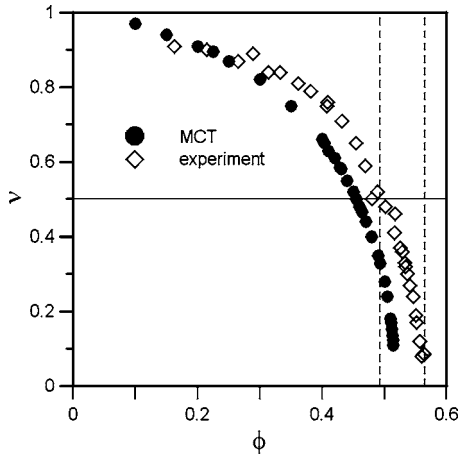

FIG. 1. Stretching index, ν, versus volume fraction, φ. The two dashed vertical lines are drawn at the first order freezing ($\varphi_f = 0.493$) and glass transition ($\varphi_g = 0.565$) volume fractions. These lines are also drawn in the remaining figures where φ is the abscissa.

the experimental result passes through the value $\frac{1}{2}$ at the (first order) freezing transition volume fraction φ_f. Figure 2 shows the connection between the MCT and experimental volume fractions for the same stretching index. The best fitting straight line through these points lies within the estimated uncertainties and passes through the origin and has a slope of 0.919. Division by the latter converts the MCT values, 0.455, where $\nu = 1/2$ and 0.516, the critical volume fraction where $\nu = 0$, into 0.495 and 0.561, respectively. Given the noise on the experimental data, no significance is presently attached to the differences between these volume fractions and those, $\varphi_f = 0.494$ and $\varphi_g \approx 0.565$, of the observed first order freezing and GT values, respectively.

In the ensuing discussion of the MCT results the volume fractions are those scaled by the factor 0.919. In addition all distances are expressed in units of the particle radius (R

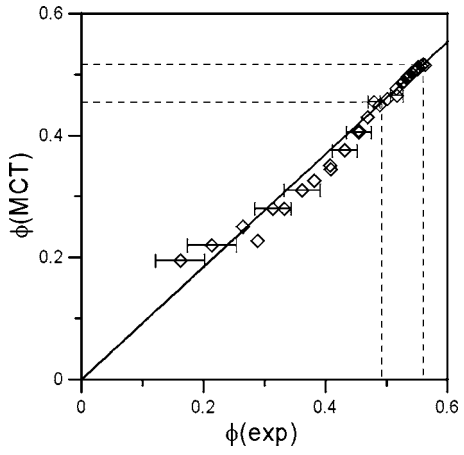

FIG. 2. MCT volume fraction versus the experimental volume fraction for the same stretching index. The solid line is the line of best fit to these data. The dashed lines correspond to the freezing and GT volume fractions, φ_f and φ_g. See text for explanation.

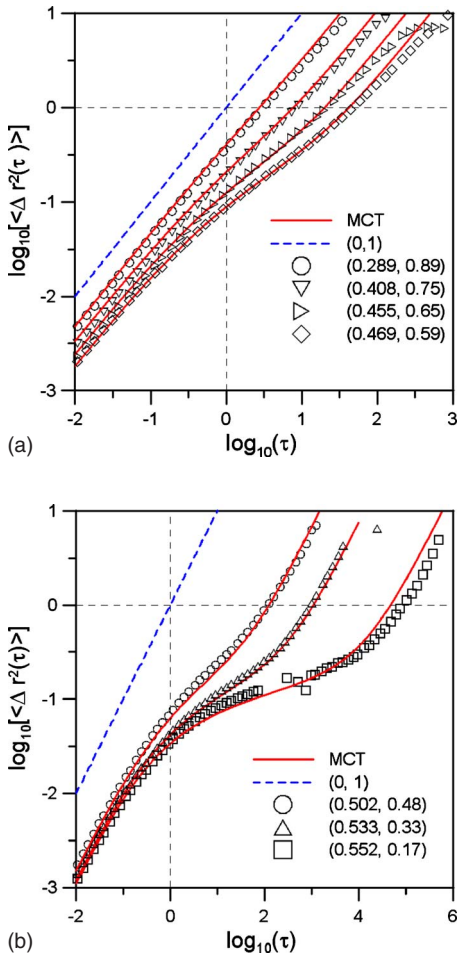

FIG. 3. (Color online) Mean-squared displacements, experiment compared with numerical MCT for volume fractions and stretching indices indicated as (φ,ν); (a) $\varphi<\varphi_f$. (b) $\varphi<\varphi_f$.

=200 nm) and delay times in terms of the Brownian characteristic time, $\tau_b=R^2/(6D_o)$.

Comparison of theoretical and experimental MSDs are shown in Figs. 3(a) and 3(b) for the thermodynamically stable ($\varphi<\varphi_f$) and metastable ($\varphi>\varphi_f$) suspensions, respectively. The results shown typify the best and the worst agreement. Since no significance can be attached to any differences with confidence, optimization of the MCT fit to the data by fine tuning the parameters has not, unlike some previous analyses [8], been exercised here.

The comparison in Fig. 3 ratifies the agreement found in previous MCT analyses of computer simulation results [20] and some of the present experimental data [10]. These analyses used the separation, ε, from φ_g as a free parameter instead of the index ν. Incidentally, they also found a linear connection between φ(exp) and φ(MCT) in the range of volume fractions, between approximately 0.5 and φ_g, where the analyses were applied. The present work shows that this consistency between the theoretical and experimental MSDs extends to arbitrarily low volume fractions.

The reduced diffusion coefficients $D^*=D_l/D_s$, where D_l and D_s are the long and short time self-diffusion coefficients [Eq. (3)] are set out against volume fraction and the stretching index in Figs. 4 and 5, respectively. In view of the uncertainties, already mentioned, the value $D^*\approx 0.08$ at φ_f is not considered as inconsistent with the empirical dynamic freezing criterion of Löwen *et al.* [26]. One also notices, in Fig. 5, that the power law, $D^*\sim\nu^5$, offers a good approximation to both theory and experiment.

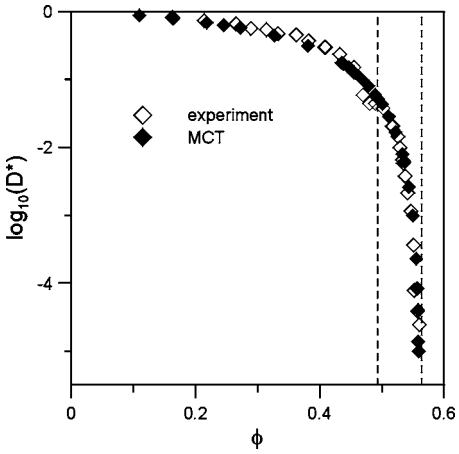

FIG. 4. Reduced diffusion coefficient versus volume fraction. See text for further details.

The delay times and root-mean-squared displacements, τ_m and R_m, at the point of maximum stretching of the MSDs are shown in Figs. 6 and 7. For $\varphi>\varphi_f$ experimental and theoretical values of τ_m and R_m are consistent. However, $\varphi<\varphi_f$ differences, not apparent in the scales used in Fig. 3, are now exposed. So, for the thermodynamically stable suspension MCT predicts the non-Markovian processes, responsible for the stretching of the MSD, to be slightly faster than seen experimentally.

Even though their microscopic time scales and the minimum logarithmic slopes of the theoretical and experimental MSDs have been matched, overlap of their respective MSDs over the whole time window is not guaranteed. So, whatever

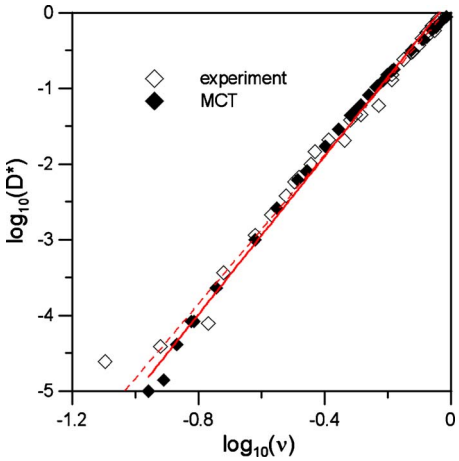

FIG. 5. (Color online) Reduced diffusion coefficient versus the stretching index. The dashed and solid lines, of slopes 4.9 and 5.2, are the best fitting straight lines through the experimental data and the MCT results, respectively.

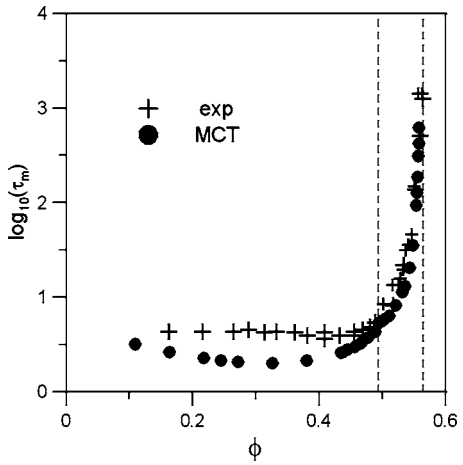

FIG. 6. Delay time, τ_m, at the point of maximum stretching of the MSD, versus volume fraction.

quantitative consistency between experiment and MCT is seen in Fig. 3, and, for that matter, in Figs. 6 and 7 is not trivial. Of course this raises the question: why is the consistency better for $\varphi > \varphi_f$ than for $\varphi < \varphi_f$?

B. Velocity autocorrelation function

A previous publication [12] shows that the VAFs of these suspensions, seen in the experimental time window, are about seven orders of magnitude smaller than the mean-squared thermal velocity, $Z(0)=\langle v^2 \rangle \approx 10^7$, and, beyond minima around $\tau \approx 10^{-2}$, they decay to the noise floor from below. However, the key feature is that the decay follows a stretched exponential function for $\varphi < \varphi_f$ and a power law for $\varphi > \varphi_f$.

As mentioned in Sec. I, in idealized MCT the microscopic dynamics are assumed to be diffusive, so its VAFs necessarily decay monotonically from below. Figure 8 shows double logarithm plots of $|Z(\tau)|$ versus τ; Fig. 8(a) for several volume fractions around φ_f; Fig. 8(b) for $\varphi > \varphi_f$; and Fig. 8(c) for $\varphi = 0.535$.

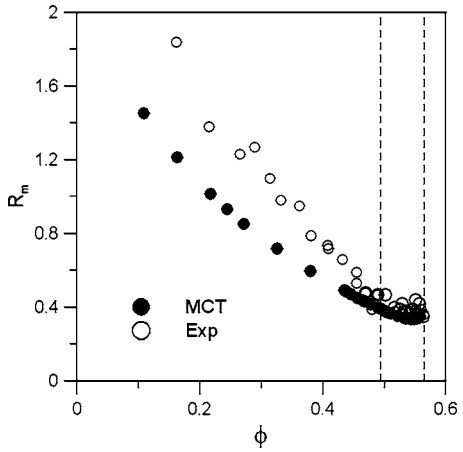

FIG. 7. Root-mean-squared displacement, R_m, at the point of maximum stretching of the MSD.

For $\varphi < \varphi_f$ one sees that a stretched exponential function,

$$Z(\tau) = -B \exp\left[-\left(\frac{\tau}{\tau_d}\right)^{\varsigma}\right], \tag{10}$$

gives a fair description of the whole decay of the VAF. The parameters of Eq. (10) that give the best fits to the numerical MCT are plotted in Fig. 9.

The values of the parameters, $B=0.5\pm0.05$, $\zeta=0.28\pm0.02$, and $\tau_d=0.008\pm0.002$, obtained by fitting Eq. (10) to the experimental VAFs [12] show no systematic variation with φ ($<\varphi_f$). The stretched exponential that best describes the experimental data for $\varphi < \varphi_f$ is also shown in Fig. 8(a). The differences between theory and experiment, displayed in Fig. 9, are that both the amplitude, B, and the decay time, τ_d, of the MCT results vary with φ. However, the stretching parameter, ζ, does not and its value agrees with the corresponding experimental result.

Around φ_f the stretched exponential fitted to the theory at long times starts to deviate at short times. These deviations increase as one proceeds deeper into the metastable regime. As demonstrated in Fig. 8(b), from the other end of the time window, the fit of Eq. (10) to the VAFs at short times deviates at long times. It is also evident that the deviation can be described by a power law,

$$Z(\tau) = -\left(\frac{\tau}{\tau_f}\right)^{-\mu}. \tag{11}$$

Figure 8(c) presents another illustration of this. Experimental and MCT VAFs for $\varphi=0.535$ (or $\nu \approx 0.33$), about midway between φ_f and φ_g, are shown. In both cases, only the initial part of the decay of the VAF is compatible with a stretched exponential. At $\tau \approx 1$ this crosses over to a power law which describes the decay of the experimental VAF down to the noise floor. For MCT there appears a time window, that expands as φ increases from φ_f to φ_g, where the VAF no longer follows a stretched exponential but can be described most simply by a power law.

The values of the parameters, $\tau_f \approx 1$ and $\mu \approx 2$, of the power law that fits the MCT results show no systematic variation with φ. The obvious difference seen in Fig. 8(c) is that the experimental result is much lower; $\tau_f \approx 0.1$. Another difference from MCT is that the observed power-law exponent, μ, varies from approximately 3/2 at $\varphi=\varphi_f$ to approximately 2 at $\varphi=\varphi_g$ [12].

Both MCT and experiment expose a difference, between the thermodynamically stable and undercooled suspensions, that warrants emphasis. First, for the thermodynamically stable suspension the experimental and MCT VAFs can both be described by stretched exponential functions of delay time, Eq. (10), with the same stretching index. As discussed elsewhere [12], this manner of decay of the VAF is fully compatible with diffusing shear modes in the suspending liquid. As mentioned in Sec. I, these mode are not included in the idealized MCT. Consequently, the velocity reversals, that necessarily result from packing constraints among the particles, are unmitigated by the delayed, positive feedback produced by the shear modes [15,16]. Herein lies a possible explanation for the quantitative differences, seen in Figs. 6

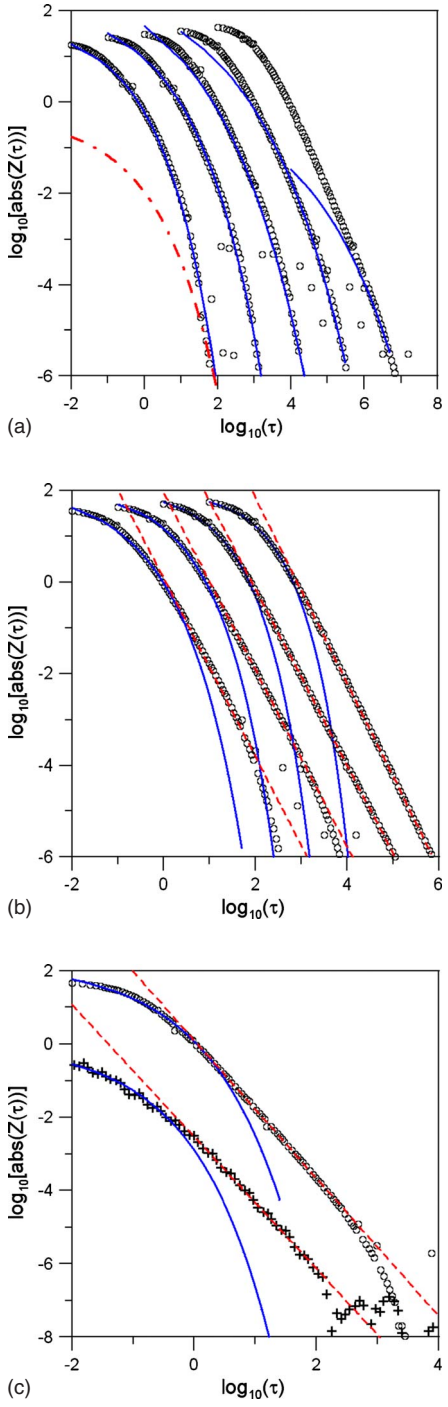

FIG. 8. (Color online) Velocity autocorrelation functions; numerical MCT indicated by circles; the stretched exponential, Eq. (10), shown by solid lines; the power law, Eq. (11), shown by dashed lines. Stray points result from amplification of numerical noise on taking the second derivative of the MSD [Eq. (7)]. (a) For values (φ,ν) from left to right, (0.438,0.65), (0.478,0.55), $(\varphi_f=0.495,0.50)$, (0.510,0.44), (0.532,0.35), with each successive result displaced along the abscissa by one; the dashed/dotted line represents the stretched exponential through the experimental data of Ref. [12]. (b) For values (φ,ν) from left to right, (0.510,0.44), (0.532, 0.35), (0.548,0.24), (0.558,0.11). (c) For (0.535,0.33). The crosses are experimental data. Take note of the changes to the scales of the axes when going from (a) to (c).

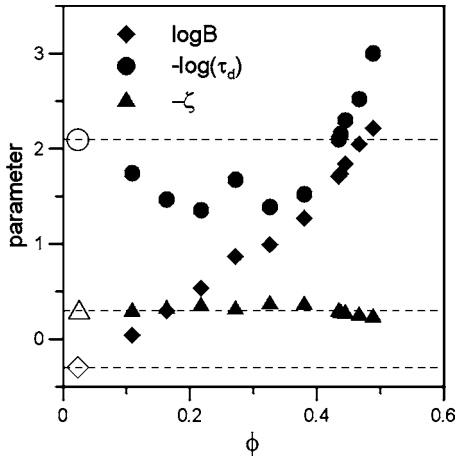

FIG. 9. Parameters of the fit of Eq. (10) to VAFs of MCT (closed symbols) and experiment (open symbols, dashed lines). See text for further details.

and 9, which indicate that the theory predicts the non-Markovian movements to be faster and the correlation of velocity reversals stronger than found experimentally.

Second, at or near the volume fraction of the first order transition the VAFs of both experiment and MCT start to show deviations from Eq. (10) that can be described most simply by a power law [Eq. (11)]. In Ref. [12] a negative algebraic decay in the VAF, where the exponent is less than $-3/2$, was read as the inability of some fraction of the particles to respond to diffusing shear modes, due to the imposition of packing constraints. In other words, in the undercooled suspension (some) particles no longer couple to those hydrodynamic modes excluded from the idealized MCT. This may be why the consistency between the theory and experiment, seen in Figs. 6 and 7, is better for $\varphi>\varphi_f$ than for $\varphi<\varphi_f$.

C. Non-Gaussian parameter

Numerical MCT results for the non-Gaussian parameter, $\alpha(\tau)$, defined in Eq. (5), are shown in Fig. 10. Figure 11 presents double logarithm plots of $\sqrt{|\alpha(\tau)|}$ and the corresponding MSDs for several volume fractions. For $\varphi<\varphi_f$ one notices that $\alpha(\tau)$ increases monotonically with τ, whereas for $\varphi>\varphi_f$ it has a minimum. Figure 12 plots the magnitude of the minimum. This is seen to extrapolate to zero at $\varphi=0.492\pm0.001$. This change in monotonicity of the non-Gaussian parameter was noted also in Ref. [19] but these authors did not draw attention to its proximity to φ_f.

Despite significant technical advances there has been little improvement, since the first attempts [27], in the accuracy of the non-Gaussian parameters measured by DLS. Typical results obtained recently [28] are shown in Fig. 13. All that can be said of these is that at very high volume fractions they also show minima and then, with increasing τ, increase without apparent limit. In these respects there is consistency with MCT. Moreover, as may be seen in Fig. 14, there is also some consistency in the location, τ_g, of the minima.

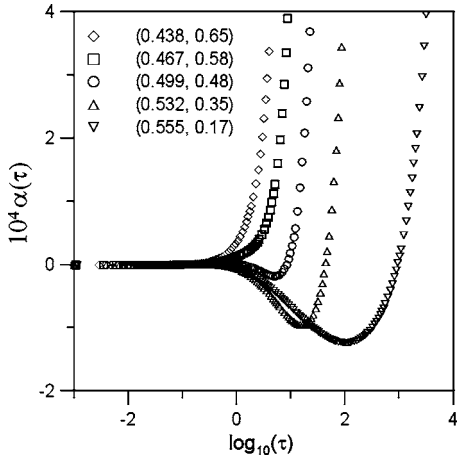

FIG. 10. Non-Gaussian parameter from MCT, for values (φ, ν) indicated.

Now according to the cumulant expansion, Eq. (2), $\alpha(\tau)$ presents the leading order deviation of the tagged particle density fluctuations from rotational invariance, i.e., $\alpha(\tau)$ is a direct measure of the symmetry breaking displacements. So it appears from Figs. 10 and 13 that symmetry breaking displacements are a necessary and ever present dynamical response to packing constraints. When φ exceeds φ_f an additional contribution emerges, one indicative of particles confined in anharmonic traps.

D. Asymptotic MCT

Reference [19] presents a detailed comparison of the asymptotic and numerical solutions of the mode-coupling equations for the self-ISF and its two leading cumulants. It is shown that the range of validity of the asymptotic results varies from one dynamical property to another and that, generally, the time window over which asymptotic and exact results coincide is significant only for very small separation, $\varepsilon = 1 - \varphi/\varphi_g$ (less than about 1%) from the GT.

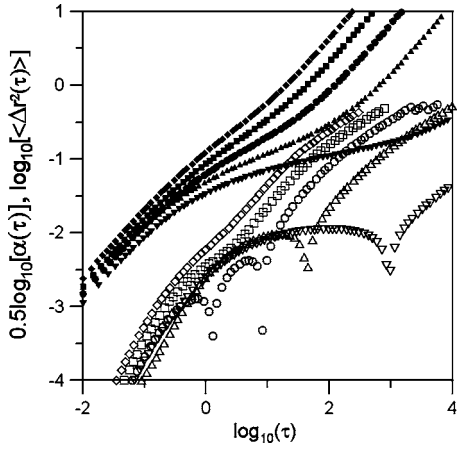

FIG. 11. Logarithm of MSD (closed symbols) and absolute value of the non-Gaussian parameter (open symbols) from MCT for pairs (φ, ν) indicated in Fig. 10.

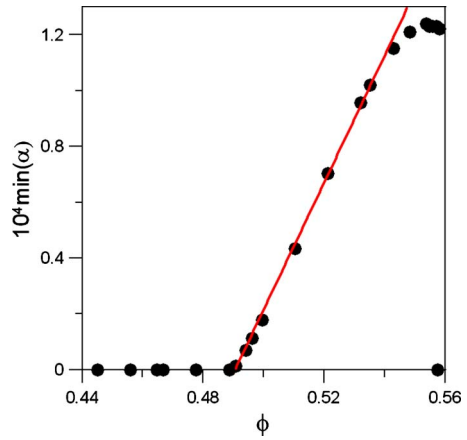

FIG. 12. (Color online) Minimum value of the non-Gaussian parameter from MCT. The line of best fit through the points between $\varphi=0.49$ and $\varphi=0.55$ extrapolates to $\min(\alpha)=0$ at $\varphi=0.491$.

There are several other ways in which the leading order asymptotic results of MCT can be tested against both the numerical MCT and experiment; these include, as discussed in Sec. II B, the predictions for the Lamb-Mössbauer factor and the scaling times of the β and α processes.

First, in Fig. 7 one sees that R_m decreases monotonically with φ up to φ_f and then shows no further systematic variation as φ approaches φ_g. Significant differences are seen between experiment and numerical MCT for $\varphi < \varphi_f$ but their respective results are more consistent for $\varphi > \varphi_f$. (The small dip in the MCT result is estimated to be within experimental noise and numerical errors incurred in the analysis of the MCT output. So, for the present discussion no significance is attached to this dip.) As mentioned in Sec. II B, the asymptotic MCT predicts the Lamb-Mössbauer factor, $f(q) = F_s^{(G)}(q, \tau_m) = \exp(-q^2 R_m^2)$, to be independent of φ. This is seen to be the case, at least approximately, for $\varphi > \varphi_f$, but definitely not for $\varphi < \varphi_f$. So this presents a point of validity of the asymptotic MCT, but only for $\varphi > \varphi_f$.

To test for the possible power-law dependence of τ_m on ε, the value of φ_g was varied until $\log \tau_m$ was found to be as

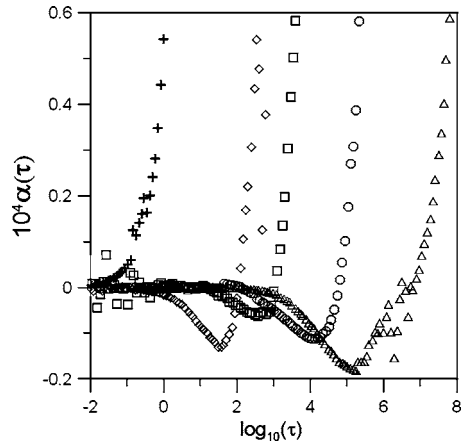

FIG. 13. Experimental non-Gaussian parameter for volume fractions, left to right, 0.29, 0.500, 0.517, 0.534, 0.560. Each successive data set is displaced along the abscissa by one.

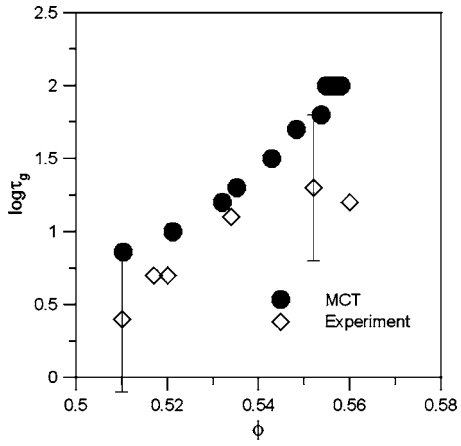

FIG. 14. Logarithm of the delay time, τ_g, at the minimum in the non-Gaussian parameter.

close as possible to a linear function of $\log \varepsilon$. Applying this procedure to the numerical MCT "data" and the experimental data, for $\varphi > \varphi_f$, required values for φ_g of 0.560 and 0.563 and yielded values of 1.6 ± 0.1 and 1.8 ± 0.2, respectively, for the values of the exponent δ in Eq. (9). The results of this analysis, shown in Fig. 15, indicate that it is possible to select values of φ_g, within the range of uncertainty of the actual values, so that τ_m follows a power-law variation with ε. Moreover, the values of the exponent then obtained, from numerical MCT and experiment, are consistent with that, $\delta = 1.66$, predicted by the asymptotic MCT for the power-law divergence of τ_β. Values of τ_β, obtained by analysis of the coherent intermediate scattering functions of the hard-sphere suspension with the asymptotic MCT [8], are also shown in Fig. 15. These results indicate equality of τ_m and τ_β and, given that, consistency with the predicted universality of τ_β.

Figure 16 plots $\log D^*$ versus $\log \varepsilon$ using the values,

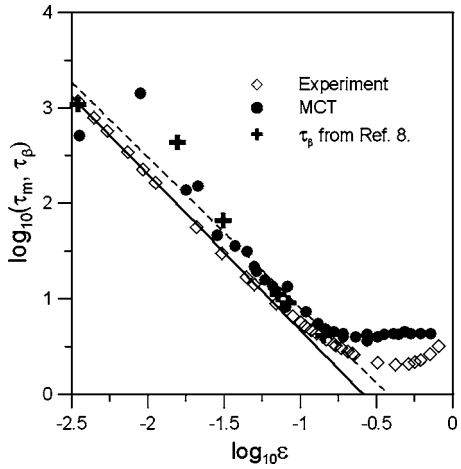

FIG. 15. Double logarithm plots of delay times, τ_m, extracted from the MCT and experimental MSDs, and the time scale, τ_β, of the β process from Ref. [8], versus the separation parameter. The solid and dashed lines represent the power laws to the MCT and experimental results. Note that $\log[\varepsilon(\varphi_f)] \approx -0.91$. See text for additional explanation.

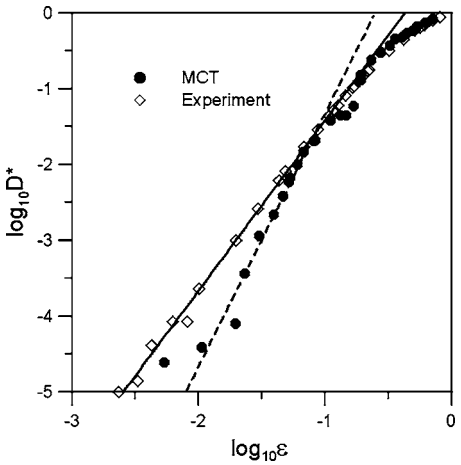

FIG. 16. Double logarithm plots of the reduced diffusion coefficient versus the separation parameter. The solid and dashed lines represent the power laws to the MCT and experimental results. See text for explanation.

0.560 and 0.563, for φ_g just obtained. The results are consistent with a power law, $(D^*)^{-1} \sim \varepsilon^{-\gamma}$ for $\varphi > \varphi_f$. Values of the exponents of the best fitting power laws are 2.2 and 3.1 for the numerical MCT and experiment, respectively. Bearing in mind the sensitivity of ε to the precise value of φ_g, the values of the exponents obtained should not necessarily be seen as grossly inconsistent with the value, $\gamma = 2.58$, predicted for the scaling time of the α process [Eq. (9)].

The consistencies that may be read from Figs. 15 and 16 between the values of τ_m and $(D^*)^{-1}$ and the power-law predictions of the asymptotic theory apply at most for $\varphi > \varphi_f$, or $\varepsilon < 0.1$. For $\varphi < \varphi_f$ deviations of the asymptotic MCT from experiment and numerical MCT cannot be rationalized by any combination of uncertainties.

Reference [11] defines the delay time τ_m as a crossover from a fast to a slow process which, so long as τ_m and τ_β are equivalent, are in turn equivalent to the β and α processes of MCT, with the amplitude of the latter being $f(q) = F_s^{(G)} \times (q, \tau_m)$. Accepting this, then in the results for τ_β and $f(q)$, obtained from experiment for $\varphi > \varphi_f$, one arrives at two of the predictions of the asymptotic MCT without, unlike previous analyses [8], direct recourse to the theory itself.

Finally, an alternative asymptotic solution [10], one based on an expansion of the memory function, m_s in Eq. (8), rather than the ISFs, reveals a contribution to the MSD proportional to $\log \tau$ infinitesimally close to the GT. This translates into a contribution to the VAF proportional to $-\tau^{-2}$. In this regard consistency is seen with the numerical MCT and experiment as $\varphi \to \varphi_g$.

IV. CONCLUSION

The numerical solutions of the idealized MCT have been compared with DLS experiments for various aspects of the tagged particle density correlator of a suspension of hard spheres. The range of volume fractions considered spans the known thermodynamically stable phase ($\varphi < \varphi_f = 0.493$) and

the undercooled, or metastable, phase ($\varphi_f < \varphi < \varphi_g \approx 0.56$) up to the GT. Alignment of the theoretical and experimental volume fractions was achieved by matching the minimum logarithmic slopes of their respective MSDs. For each φ the measured short time self-diffusion coefficient was then factored into the MCT result to bring its time scale into alignment with the experimental one. This rescaling brings the theoretical and experimental MSDs and the long-time self-diffusion coefficients of MCT into quantitative agreement for the whole range of volume fractions ($0.2 < \varphi_g$) studied experimentally. So, on the face of it, MCT quantitatively describes the experimental MSDs, not just near φ_g, as expected from the asymptotic solutions, but for all φ on the fluid side of the GT at least.

The most intriguing outcome of MCT is the emergence of nonmonotonicity in the non-Gaussian parameter and the appearance of negative algebraic decays in the VAF. That these occur at the volume fraction, φ_f, of the first order transition, or as close to φ_f as experimental noise and resolution allow one to specify, may be just a coincidence, a coincidence possibly peculiar to a system of diffusing hard spheres. However, given the consistency of experiment and MCT with regard to the VAF at least, it is nonetheless a curious coincidence, made all the more so by the results of molecular dynamics simulations of (Newtonian) hard spheres which indicate the disappearance, from the dynamical window, of the (positive) $\tau^{-3/2}$ hydrodynamic power law (the manifestation of diffusing transverse momentum) and the emergence of a negative, $-\tau^{-5/2}$, power law in the VAF at φ_f precisely [13]. Moreover, simulations of a binary mixture of hard spheres find that this exchange of positive and negative algebraic decays of the VAF occurs at the known freezing volume fraction of that mixture.

In Ref. [12] a negative algebraic decay in the VAF, where the exponent is less than $-3/2$, was attributed to the presence of particles whose response to thermal forces is impaired because they are indefinitely trapped in clusters ("indefinitely" meaning the time while the metastable fluid maintains its integrity—there being no evidence of nucleation). The picture of such dynamical heterogeneity—clusters of particles immersed in a sea of comparatively mobile particles—is well-known from optical microscopy [29,30] and computer simulations [31] of very dense suspensions and molecular fluids. So, it appears that for volume fractions greater than φ_f the impost of packing constraints is such that particles start to trap themselves in clusters which, as shown recently, may percolate the system [30]. As schematized and discussed in Ref. [32] force chains that may be present in these clusters provide a fragile resistance to low frequency shear stresses. In this we see a possible route to vitrification.

But could there be another role for these clusters of particles? Is it plausible that, in response to whatever stresses the mobile interstitial material exerts on the clusters, Bragg reflecting crystals are formed through registration of the force chains into layers and then stacks. Consider the results of recent experiments on the crystallization kinetics of these hard-sphere suspensions [33]. These indicate the presence, immediately after shear melting, of compressed amorphous or smectic structures [34] whose average linear dimension of some 15 particle diameters shows little variation with either volume fraction or the spread in particle radii. It also has become evident that conversion to the crystalline phase—the emergence of those reflections indicative of hexagonal packing—is initiated from these structures [33]. Moreover, the compactness of these precursors means that even a small spread in particle radii (say, around 5% of the mean) demands some local fractionation for the registration processes to occur [35]. Indeed, even if inadvertently, size polydispersity in these suspensions has been exploited in order to delay the induction of the crystalline solid and protract the metastable state without, as evident from the results in Ref. [7], significant impact on the particle number density fluctuations.

So, the proposal is that at volume fractions exceeding φ_f, irrespective of the microscopic dynamics, packing constraints are so severe that particles become trapped in clusters. Percolation of the clusters leads to solidification in an amorphous state while organization, or registration, within the clusters initiates solidification in the crystalline state.

If one accepts the above interpretation of the qualitative change in the VAF at φ_f then MCT must be seen in a broader context. Indeed the mode coupling equations, as formulated in Refs. [1,2], to describe structural relaxation in dense fluids possess a dynamical singularity. Asymptotic solutions about this singularity describe the slowing of density fluctuations and their partial arrest in a manner that agrees with observations, at least for some simple glass formers (asymptotically) near their respective glass transition points. So, from the perspective of the asymptotic solutions alone MCT is, at most, a theory for the glass transition. However, the above analysis, on the basis of the complete numerical solutions, suggests the delayed, nonlinear feedback in the mode coupling equations also encapsulates a degree of subtlety that has so far gone unnoticed: the cooperation that distinguishes the dynamics of thermodynamically stable and undercooled hard-sphere suspensions and, in the latter, the cooperation that sets up the structural precursors for the first order freezing transition.

ACKNOWLEDGMENTS

My thanks go to M. R. Mayr for providing the numerical solutions of the MCT and to G. Bryant, H. J. Schöpe, M. Sperl, and Th. Voigtmann for comments on the manuscript.

[1] E. Leutheusser, Phys. Rev. A **29**, 2765 (1984); U. Bengtzelius, W. Götze, and A. Sjölander, J. Phys. C **17**, 5915 (1984).
[2] W. Götze, J. Phys.: Condens. Matter **11**, A1 (1999).
[3] J. Frenkel, *Kinetic Theory of Liquids* (Oxford University Press, Oxford, 1946).
[4] J. C. Maxwell, Philos. Trans. R. Soc. London **157**, 49 (1867).
[5] P. N. Pusey and W. van Megen, Nature (London) **320**, 340 (1986).
[6] W. van Megen and S. M. Underwood, Nature (London) **362**, 616 (1993).
[7] S. I. Henderson *et al.*, Physica A **233**, 102 (1996) S. I. Henderson and W. van Megen, Phys. Rev. Lett. **80**, 877 (1998).
[8] W. van Megen and S. M. Underwood, Phys. Rev. E **47**, 248 (1993); **49**, 4206 (1994).
[9] W. van Megen, T. C. Mortensen, S. R. Williams, and J. Muller, Phys. Rev. E **58**, 6073 (1998).
[10] M. Sperl, Phys. Rev. E **71**, 060401(R) (2005).
[11] W. van Megen, T. C. Mortensen, and G. Bryant, Phys. Rev. E **72**, 031402 (2005).
[12] W. van Megen, Phys. Rev. E **73**, 020503(R) (2006); W. van Megen and G. Bryant, *ibid.* **76**, 021402 (2007).
[13] S. R. Williams, G. Bryant, I. K. Snook, and W. van Megen, Phys. Rev. Lett. **96**, 087801 (2006).
[14] M. H. Ernst and A. Weyland, Phys. Lett. **34A**, 39 (1971).
[15] B. J. Alder and T. E. Wainwright, Phys. Rev. A **1**, 18 (1970); M. H. Ernst, E. H. Hauge, and J. M. J. van Leeuwen, *ibid.* **4**, 2055 (1971); J. R. Dorfman and E. G. D. Cohen, *ibid.* **6**, 776 (1972).
[16] J.-P. Hansen and I. R. McDonald, *Theory of Simple Liquids* (Academic Press, London, 1986).
[17] J. P. Boon and S. Yip, *Molecular Hydrodynamics* (Dover, Toronto, 1980).
[18] P. N. Pusey, in *Liquids, Freezing and the Glass Transition*, edited by J.-P. Hansen, D. Levesque, and J. Zinn-Justin (North-Holland, Amsterdam, 1991), p. 763.
[19] M. Fuchs, W. Götze, and M. R. Mayr, Phys. Rev. E **58**, 3384 (1998).
[20] Th. Voigtmann, A. M. Puertas, and M. Fuchs, Phys. Rev. E **70**, 061506 (2004).
[21] W. van Megen and S. M. Underwood, J. Chem. Phys. **91**, 552 (1989).
[22] B. R. A. Nijboer and A. Rahman, Physica (Amsterdam) **32**, 415 (1966).
[23] W. G. Hoover and F. H. Ree, J. Chem. Phys. **49**, 3609 (1968).
[24] S. M. Underwood, J. R. Taylor, and W. van Megen, Langmuir **10**, 3550 (1994).
[25] M. R. Mayr (private communication).
[26] H. Löwen, T. Palberg, and R. G. Simon, Phys. Rev. Lett. **70**, 1557 (1993).
[27] W. van Megen and S. M. Underwood, J. Chem. Phys. **88**, 7841 (1988).
[28] Some of these results derive from T. C. Mortensen, Ph.D. thesis, RMIT, 2002 (unpublished).
[29] W. K. Kegel and A. van Blaaderen, Science **287**, 290 (2000); E. R. Weeks *et al.*, *ibid.* **287**, 627 (2000).
[30] J. C. Conrad, P. P. Dhillon, E. R. Weeks, D. R. Reichman, and D. A. Weitz, Phys. Rev. Lett. **97**, 265701 (2006).
[31] W. Kob, J. Phys.: Condens. Matter **11**, R85 (2000); S. C. Glotzer, J. Non-Cryst. Solids **274**, 342 (2000).
[32] M. E. Cates, J. P. Wittmer, J. P. Bouchaud, and P. Claudin, Phys. Rev. Lett. **81**, 1841 (1998).
[33] H. J. Schöpe, G. Bryant, and W. van Megen, Phys. Rev. Lett. **96**, 175701 (2006).
[34] S. Martin, G. Bryant, and W. van Megen, Phys. Rev. Lett. **90**, 255702 (2003).
[35] S. R. Williams, I. K. Snook, and W. van Megen, Phys. Rev. E **64**, 021506 (2001).